Supplementary Information to accompany

No ion is an island: Multiple ions influence boron incorporation into $CaCO_3$

by

Henehan, Michael J., Klein Gebbinck, Christa D., Wyman, Jillian V. B., Hain, Mathis P., Rae, James W. B., Hönisch, Bärbel, Foster, Gavin L. and Kim, Sang-Tae.

Supplementary Information includes:

Supplementary Figures 1 – 14

Supplementary Animation 1 *(GIF file, downloadable separately. Caption included here.)*

Supplementary Tables 1 – 3 *(Excel files downloadable separately)*

Supplementary Appendix 1: Sanyal et al. (2000) reanalysis (*incl. Figs A1, A2*)

Supplementary Appendix 2: X-ray Diffraction spectra from synthetic precipitates

a. Aragonites

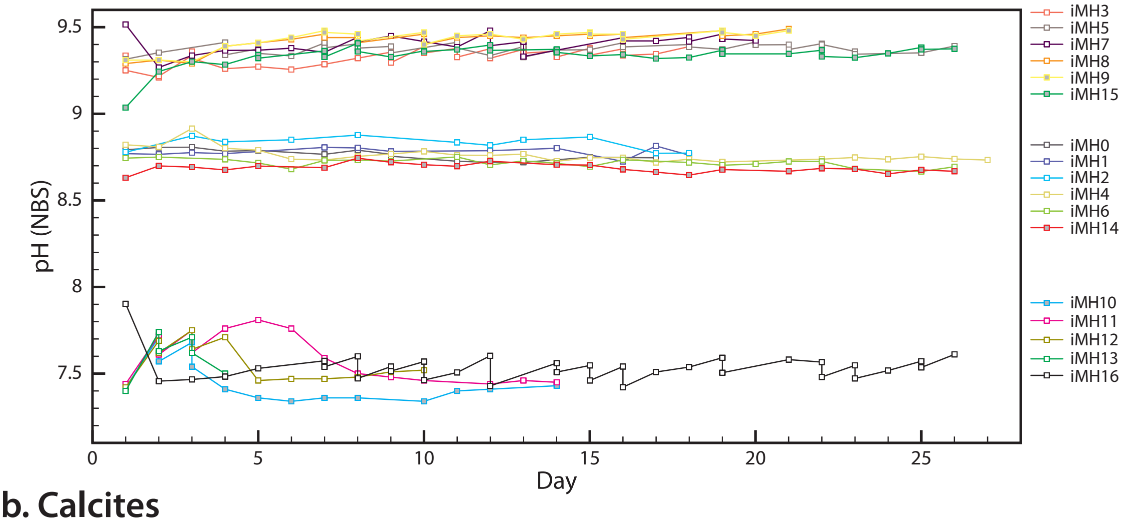

b. Calcites

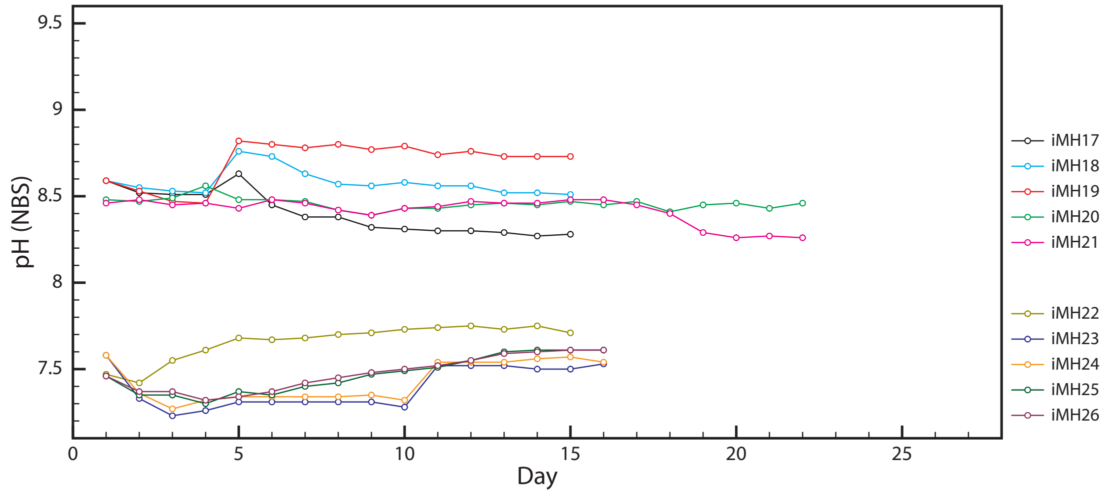

Supplementary Fig. 1: *Near-daily pH measurements taken during our experiments. In some experiments, pH was occasionally adjusted by addition of HCl / NaOH to minimize drift- in these cases the pH before and after adjustment is shown. Since the sampled carbonate averages out the variability in pH, quoted uncertainty on pH for each experimental datapoint is two standard errors of the mean of the pH measurements during precipitation. In the cases where pH was adjusted by NaOH/HCl addition, both the pre-adjustment and post-adjustment values are included in calculation of the mean and standard error on the mean. Raw data are provided in Supplementary Table 3.*

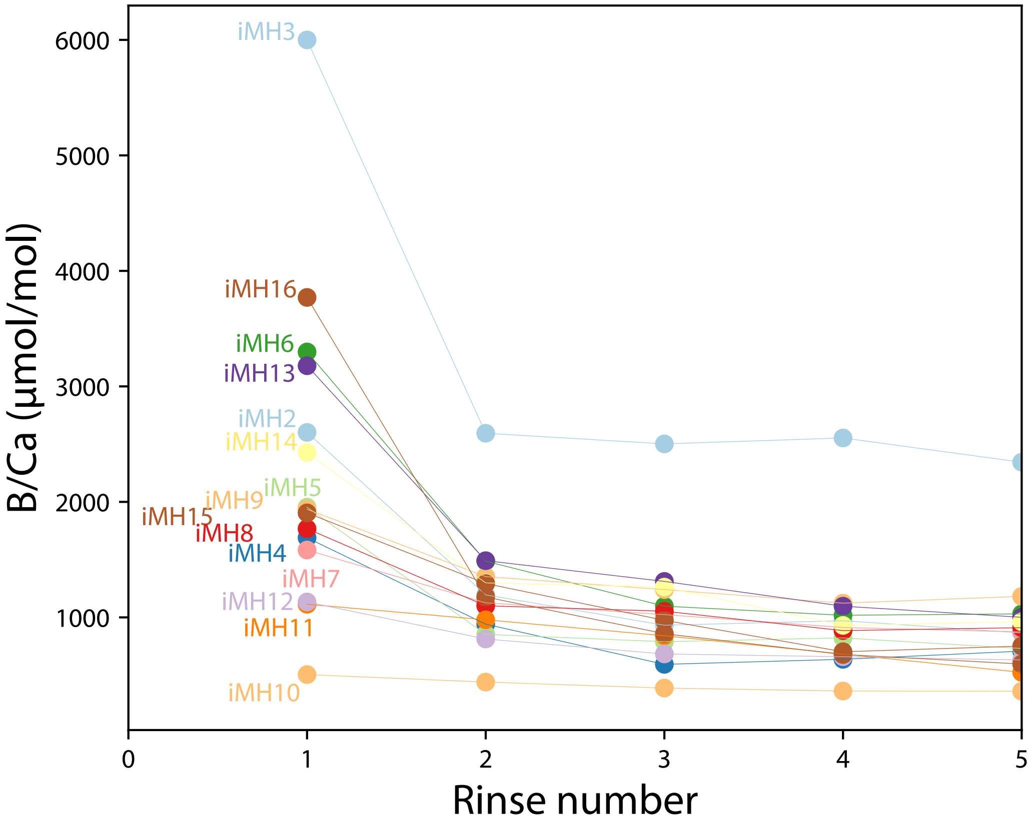

Supplementary Fig. 2: *For a subset of our synthetic carbonates, five rinses in Milli-Q 18.2 Ω water was analysed on a Thermo X-Series II at the University of Southampton, to ensure that samples were adequately rinsed to remove all adsorbed B. Note that this follows the initial wash with 2 L of B-Free H_2O after separation from the precipitation medium. Furthermore, after these 5 rinses, a further 3 rinses were carried out before the sample was dissolved for analysis. Note this analysis was carried out for only a subset of the data, after which the same cleaning protocol was deemed sufficient for other samples.*

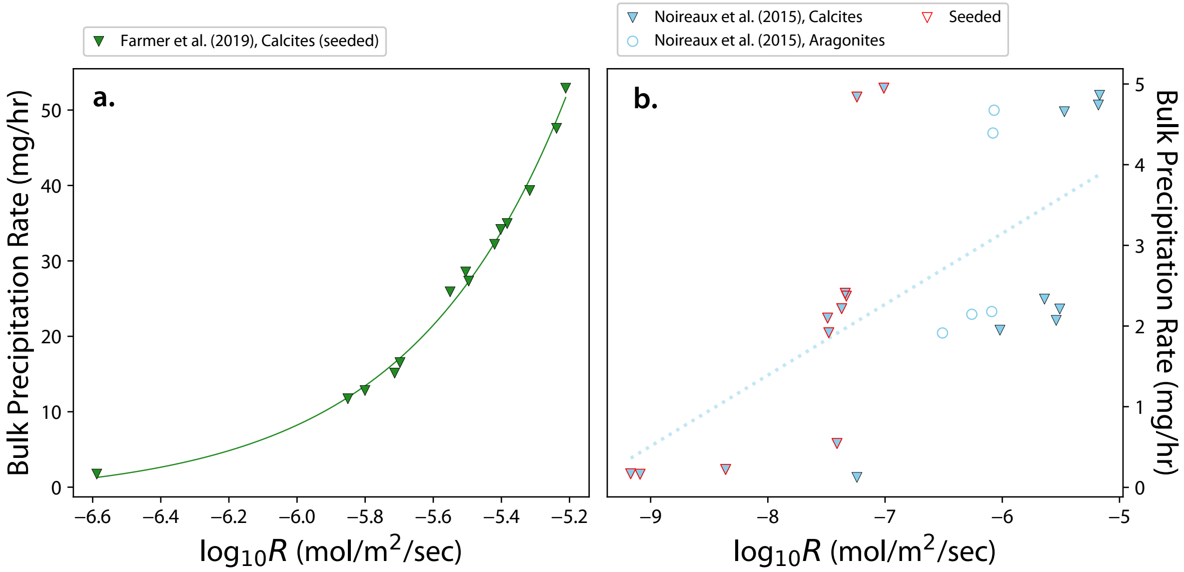

Supplementary Fig. 3: *In both Farmer et al. (2019, panel a) and Noireaux et al. (2015, panel b), surface-area normalized precipitation rate was reasonably well correlated with bulk precipitation rate- suggesting our use of this metric should be largely reliable.*

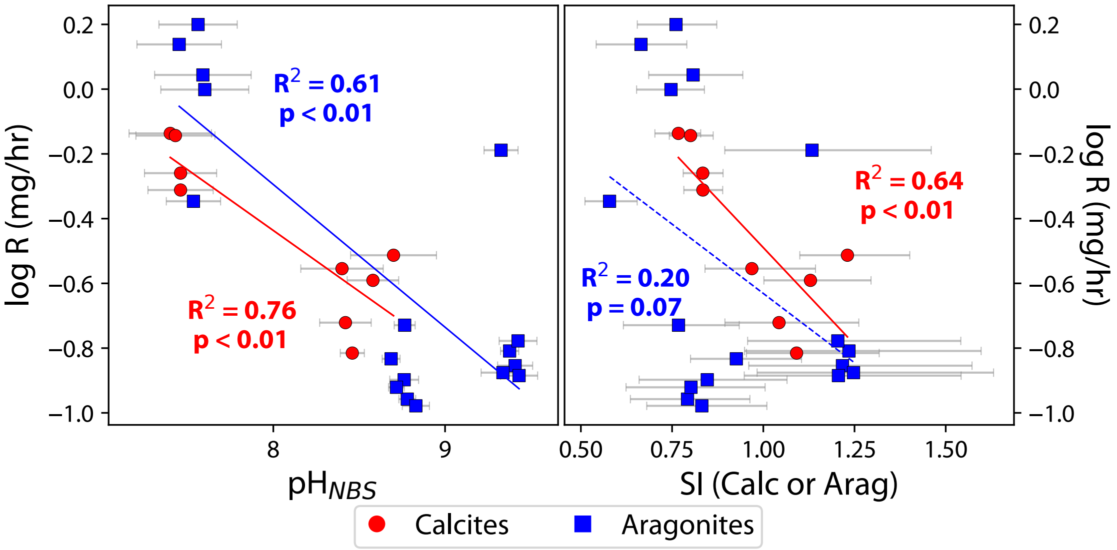

Supplementary Fig. 4: *Although counterintuitive, pH and saturation index (SI) are anti-correlated with bulk precipitation rate in our experiments, for both polymorphs. This may suggest that the higher [Ca] in lower pH experiments accelerated $CaCO_3$ precipitation more than one might expect from its effect on SI alone. This highlights that using SI to derive precipitation rate (as done by Farmer et al. 2019) would not be appropriate for this dataset.*

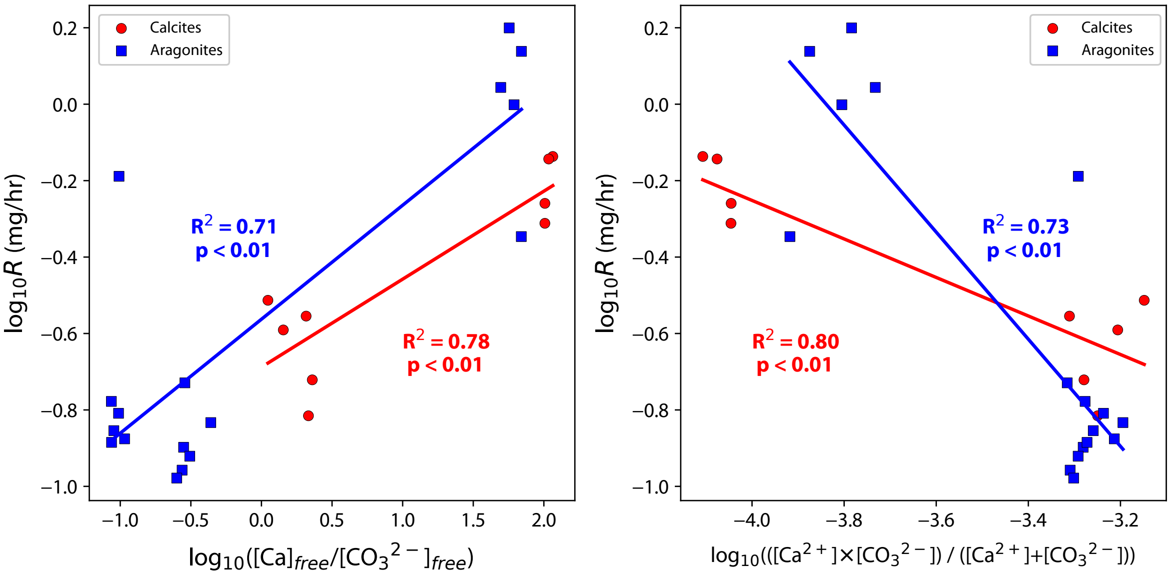

Supplementary Fig. 5: *In our experiments the ratio of calcium to carbonate ion in our growth media (panel a) is correlated strongly with bulk precipitation rate, confirming suggestions of Nehrke et al. (2007) and van der Weijden and van der Weijden (2014). Similarly, considering the product/sum of $CaCO_3$ is also a strong predictor (as suggested by Evans et al. 2020).*

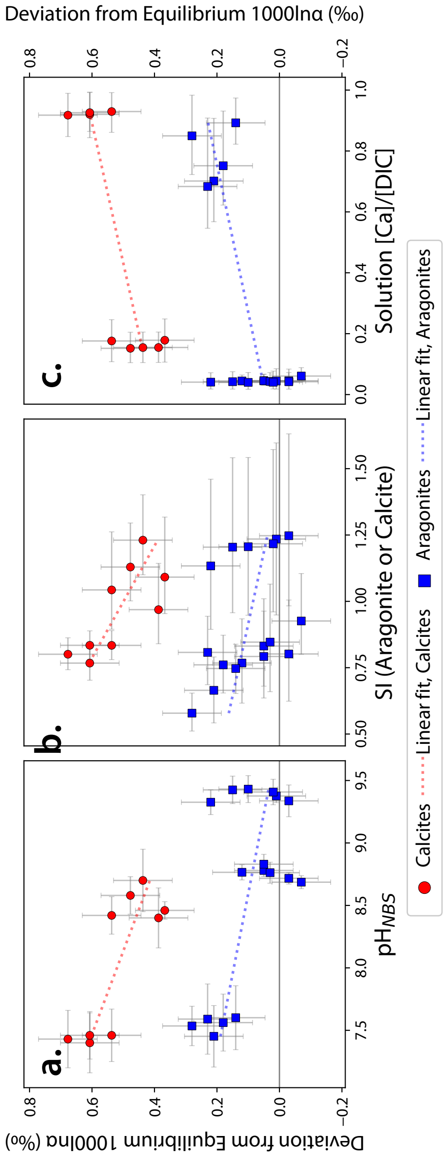

Supplementary Fig. 6: *Degree of oxygen isotope disequilibrium relative to each polymorph's respective equilibrium value (from Kim and O'Neil, 1997; Kim et al., 2007) is not strongly correlated with any one solution chemistry parameter. In our experiments, [Mg]:[Ca] was kept at a constant ratio within calcites (1.3:10) or aragonites (4:1), with concentrations of each adjusted to reach approximately similar rates of precipitation. Thus, although high pH conditions (a) produce high calculated SI (b), where one would perhaps predict a higher likelihood of kinetic isotope effects, these conditions produce lnα values closer to equilibrium. If anything, the increase of [Ca] relative to [DIC] required to maintain similar rates of precipitation at low pH seems most clearly linked to oxygen isotope disequilibrium (c), but again, the correlation is weak. Error bars are quadratic addition of 1σ reproducibility on oxygen isotope analyses of solid and solution (y-error, all panels), two standard deviations of in-run pH measurements (panel a), 95% quantiles on 2000 Monte Carlo simulations of SI (panel b) or [Ca]/[DIC] (panel c), taking into account major ion concentration and carbonate system change within run.*

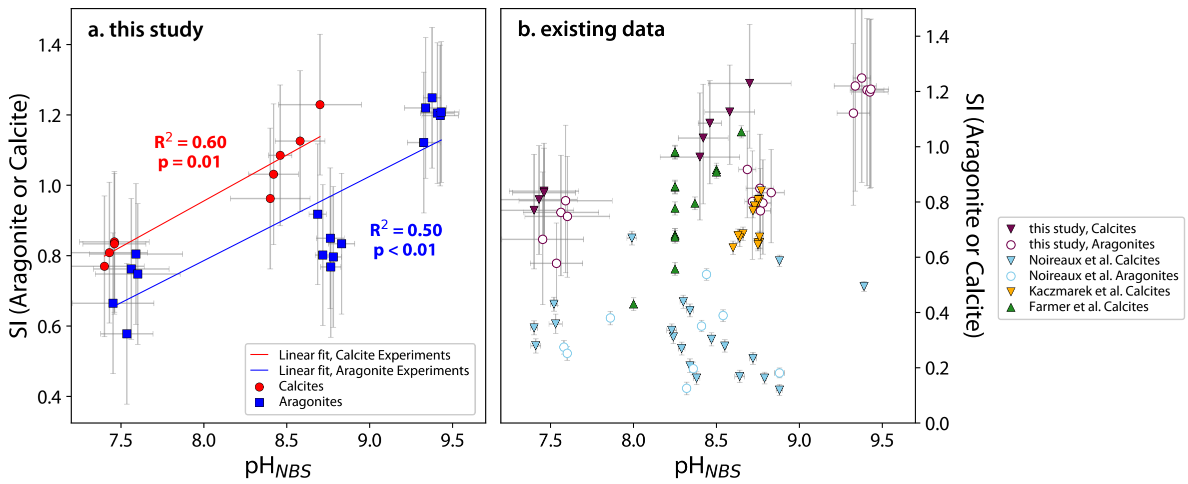

Supplementary Fig. 7: *Although we intended to maintain approximately constant saturation and precipitation rates across experiments, decoupled from pH change, pH and SI are correlated in our dataset. This is also seen in other published calcite datasets, but not in the experiments of Noireaux et al. (panel b). Error bars on our experimental SI data are based on 95% quantiles of 2,000 Monte Carlo simulations, each with simulated uncertainty in pH and major ion chemistry. Linear fits are the median slopes and intercepts of regression lines through each of these Monte Carlo simulated datasets, and R^2 and p values are similarly the median values of these parameters for each Monte Carlo regression.*

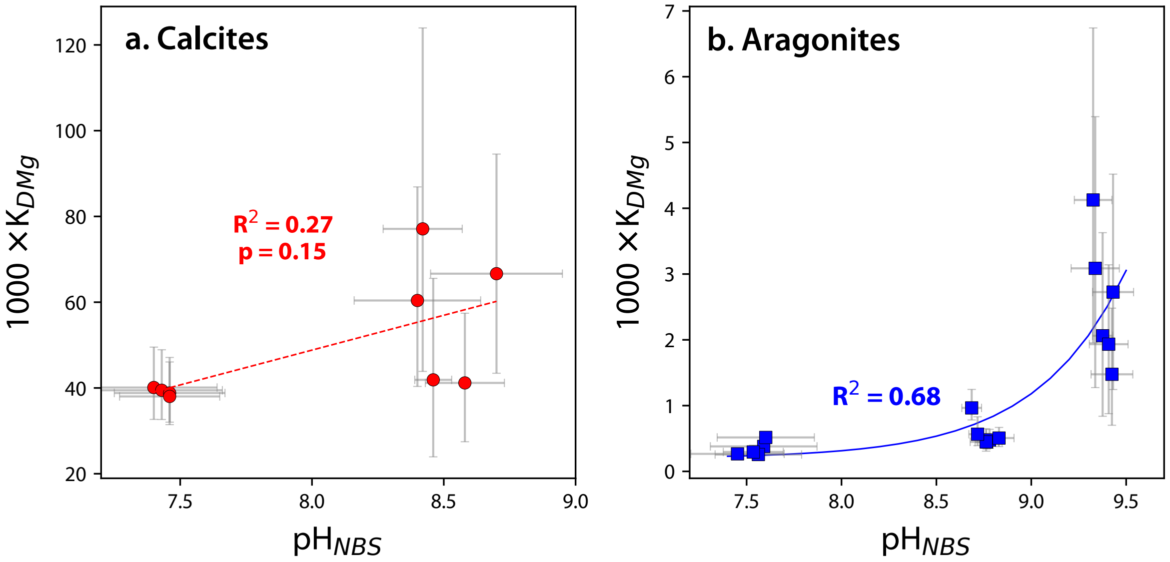

Supplementary Fig. 8: *Incorporation of Mg in calcite (panel a) and aragonite (panel b) increasing as a function of pH. Data is the same as in Fig. 2, but shown here on a linear scale.*

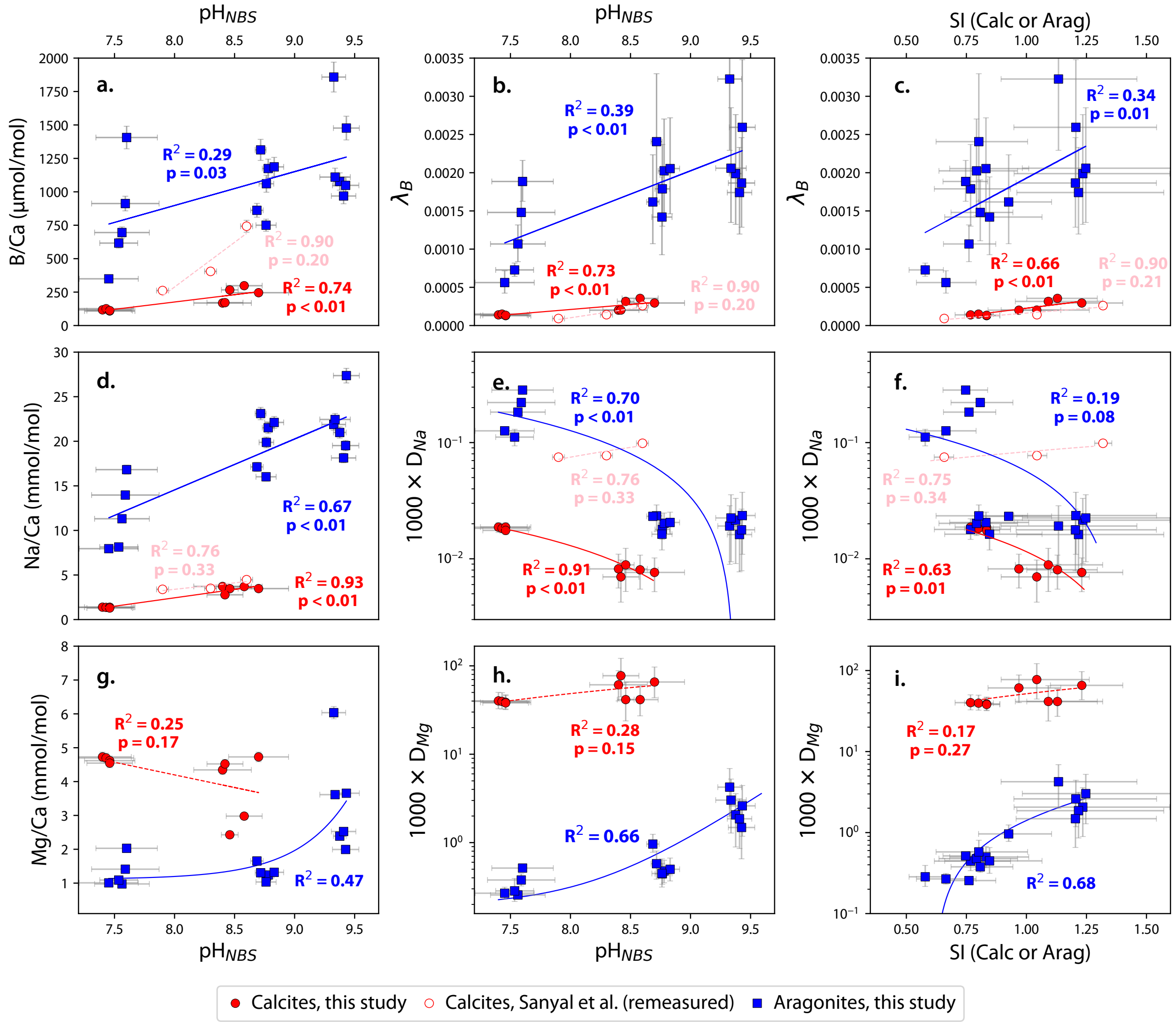

Supplementary Fig. 9: *As in Fig. 2 (main text), the observed response of B, Na and Mg incorporation to changes in the carbonate system, but including the remeasured data from Sanyal et al. (2000)'s precipitates. Both B/Ca (panel a) and Na/Ca (panel d) ratios increase with pH in our aragonites (blue squares) and calcites (red circles), and Sanyal et al.'s calcites (pink circles). Because B/DIC did not vary significantly in the experiments, this is equally evident in* λ_B *values* ($\lambda_B = B/Ca_{carbonate} / ([B]_{solution}/[DIC]_{solution})$)*, shown in panel e. By contrast, considering the changing Na/Ca of solution, partitioning of Na into the solid form* (D_{Na}) *decreases in our carbonates when pH is higher (panel e), but increases in the calcites of Sanyal et al. (2000). This may reflect the fact that for Sanyal et al.'s experiments, pH correlates positively with precipitation rate, but for our experiment it is negatively correlated (see Supp. Fig. 4).*

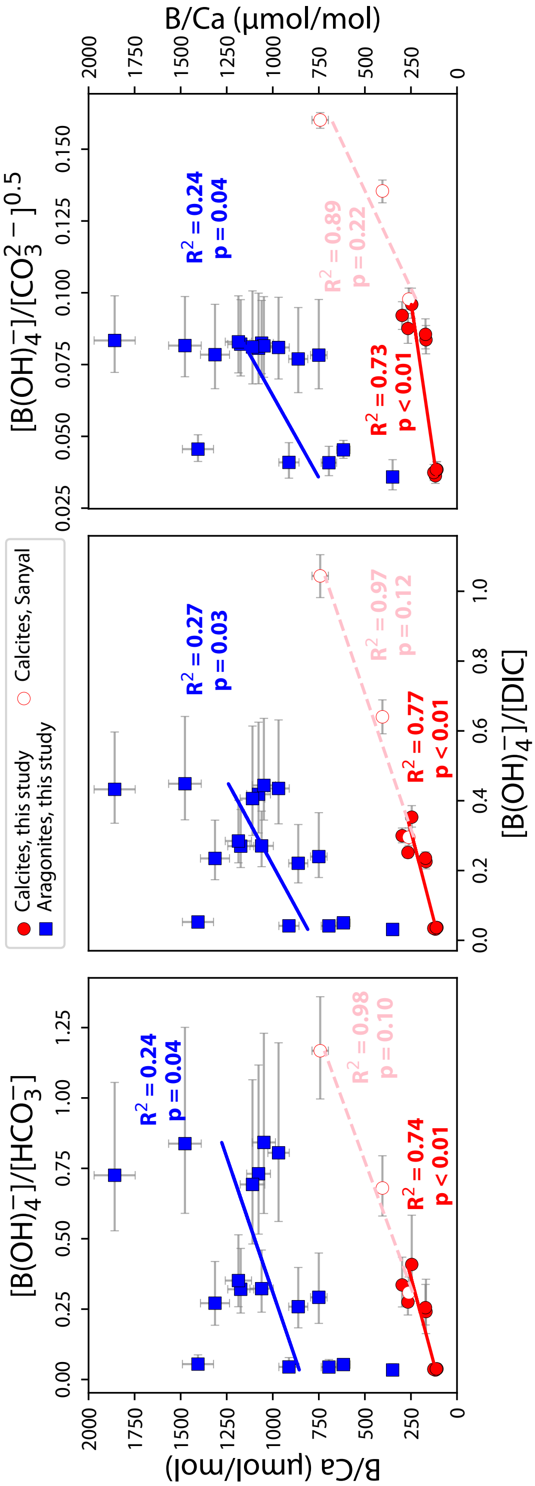

Supplementary Fig. 10: *There is no significant improvement in fit (and indeed for aragonite, there is some deterioration) when plotted against other borate-carbonate system parameters, as calculated via PHREEQC, and so we plot against pH (as the least derived parameter) in the main text Fig. 2. Error bars on x-axis variables are based on 95% quantiles of 2,000 Monte Carlo simulations, each with simulated uncertainty in pH and major ion chemistry, and R^2 and p values are similarly the median values of these parameters for each Monte Carlo regression. Error bars on B/Ca are 6% external reproducibility based on long term repeat measurements of standards. The consistency of our calcites with Sanyal et al. (2000)'s calcites when plotted in Borate/DIC space may speak against the universal applicability of λ_B, as used by Uchikawa et al. (2015, 2017).*

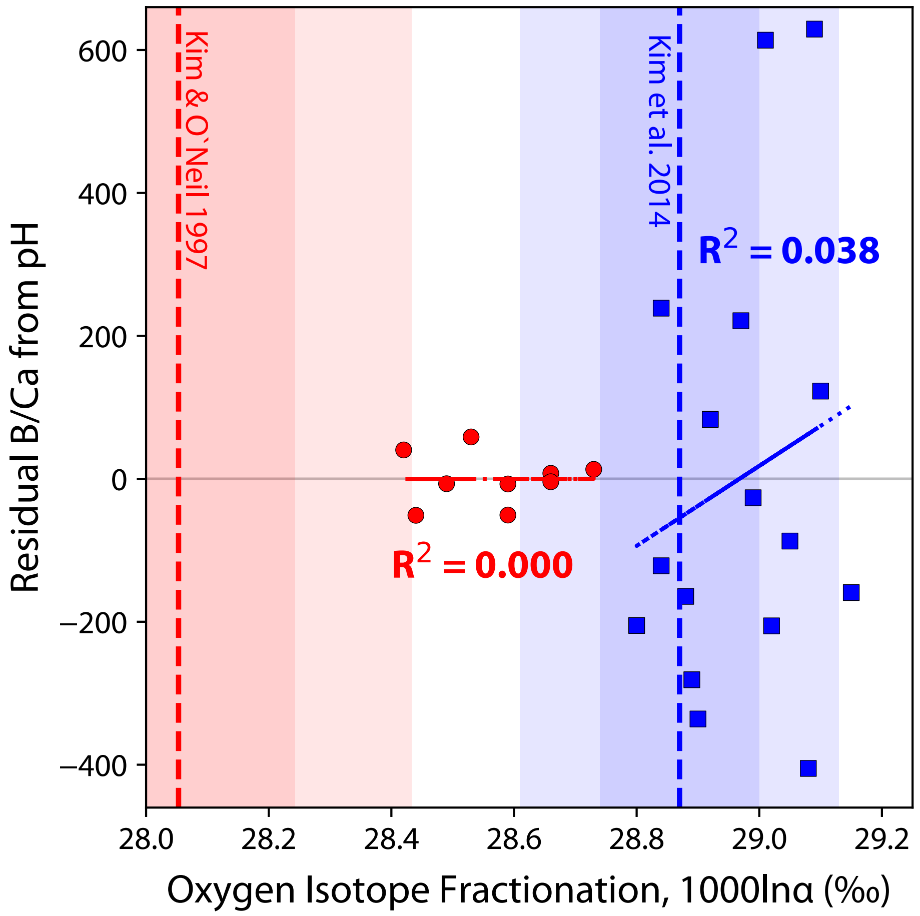

Supplementary Fig. 11: *Residual scatter around our B/Ca-pH relationships for calcite (red circles) and aragonite (blue squares) is not correlated with variability from oxygen isotope equilibrium (plotted as dashed lines for each polymorph).*

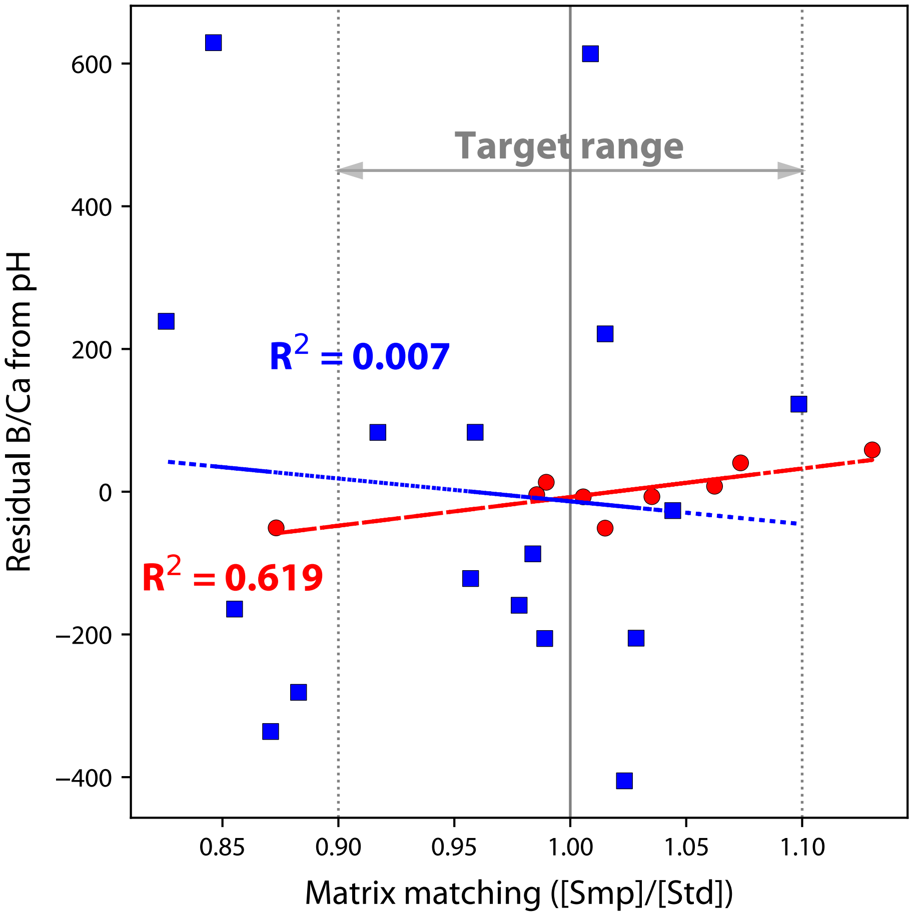

Supplementary Fig. 12: *Although every attempt was made to match sample and standard concentration during B/Ca ICPMS analysis, some samples did fall outside of the ±10% range normally targeted for measurement. Although there is a significant correlation within sampled calcites (red) between offset from the B/Ca-pH relationship and matrix matching, that could indicate some analytical concern for these two datapoints, no such correlation is evident for aragonites (blue). Therefore, since any effects of sample-standard matrix-mismatching should be independent of carbonate polymorph, unless there is some additional confounding and fundamentally different secondary driver of B/Ca variability in aragonite, we suggest that analytical issues are unlikely to be the source of the considerable scatter in our B/Ca data.*

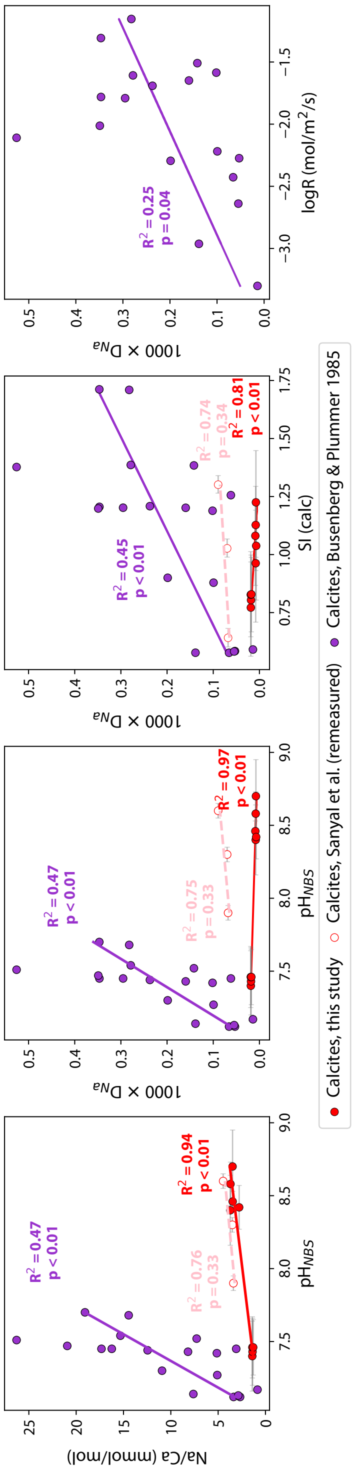

Supplementary Fig. 13: *Data from aragonite precipitates of Busenberg and Plummer (1985), which demonstrate similar, or indeed stronger, positive correlations between Na incorporation (either raw Na/Ca or D_{Na}, defined as $(Na/Ca_{carbonate})/([Na]_{sol}/[Ca]_{sol})$) and carbonate chemistry parameters. While also correlated with precipitation rate (calculated from the mg/min precipitated per g of seed, and a surface area of the seed material of $0.6 m^2/g$), the correlation is weaker than against carbonate system conditions. Note that since most of the DIC that is present in the solutions of Busenberg and Plummer (1985) is in the form of HCO_3^-, formulation as K_D $((Na/Ca_{carbonate})/([Na]_{sol}/[HCO_3^-]_{sol}))$, is indiscernibly different.*

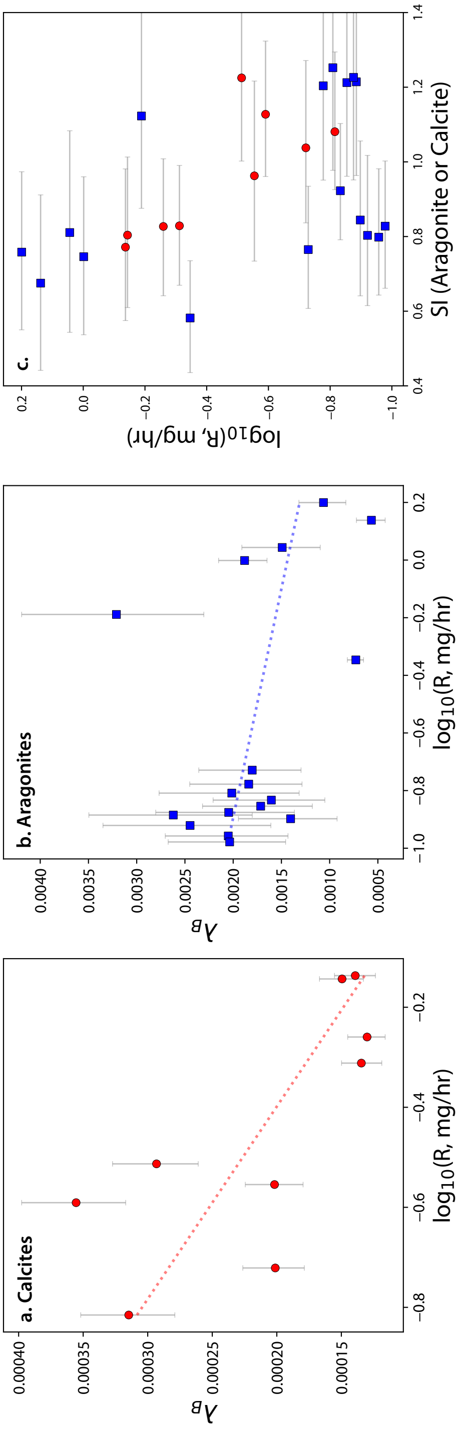

Supplementary Fig. 14: *Assuming our bulk precipitation rate metrics are reasonable approximations of crystal growth rate, if anything higher precipitation rate equates to lower λ_B values.*

Caption to Supplementary Animation 1: Animated multiple linear regression model from Fig. 8 (main text), rotating for ease of visibility of residual variability around the model.

Supplementary Appendix 1: Reanalysis of calcites precipitated by Sanyal et al. (2000)

Subsamples of the calcites from Sanyal et al. (2000)'s original experiments were reanalyzed at the University of Bristol in 2010, following the analytical protocols laid out in Foster (2008) and Rae et al. (2011). Samples were cleaned prior to dissolution to remove any residual solution or other surface contaminants. Specifically, around 1 mg of each sample powder was placed into acid-cleaned plastic centrifuge tubes, and rinsed three times in B-free Milli-Q water (18.2 MΩ), ultrasonicating each time. These rinses were collected for elemental analysis. MilliQ rinses were followed by a weak acid leach in 0.0005 M HNO_3 for 1 minute, and three further rinses in MilliQ. Cleaned samples were dissolved in distilled 0.075 M HNO_3, and an aliquot of dissolved solution was set aside for elemental analysis. Boron was then separated from the carbonate matrix by ion exchange chromatography with Amberlite 743 following the procedures described in Foster (2008).

Elemental analyses (initial rinses and carbonates) were made on an Element 2 HR-ICPMS following established protocols (Ni et al. 2007). Boron isotope analyses were made on a Neptune MC-ICPMS following Foster (2008) and Rae et al. (2011). Uncertainty on these boron isotope analyses was estimated as two standard deviations of 4 replicate analyses (from two different column separations).

Unfortunately, as can be seen in Fig. A1 below, B/Ca ratios in rinses 1-3 have still not plateaued at low consistently low values, nor do the values of B/Ca approach those of the carbonate solid phase, suggesting there was still non-negligible amounts of B from the growth medium adsorbed to the calcites after 3 rinses. Given the observations we made in our later experiments (Supp. Fig. 2), where more rinse steps were tested, it is highly likely that after a weak acid leach and three more Milli-Q rinses, this remaining adsorbed B would have been removed from the carbonates. However, we cannot be certain that this is the case. Therefore, we present these data in this paper with the caveat that we cannot be fully certain that all growth medium B was removed prior to dissolution. The good agreement between our new calcite data and these remeasured Sanyal et al. (2000) precipitates when plotted in B/Ca vs. $[B(OH)_4^-]/[DIC]$ space (Supp. Fig. 10) gives us some confidence that cleaning was sufficient, but we recognize that this is a post-hoc evaluation.

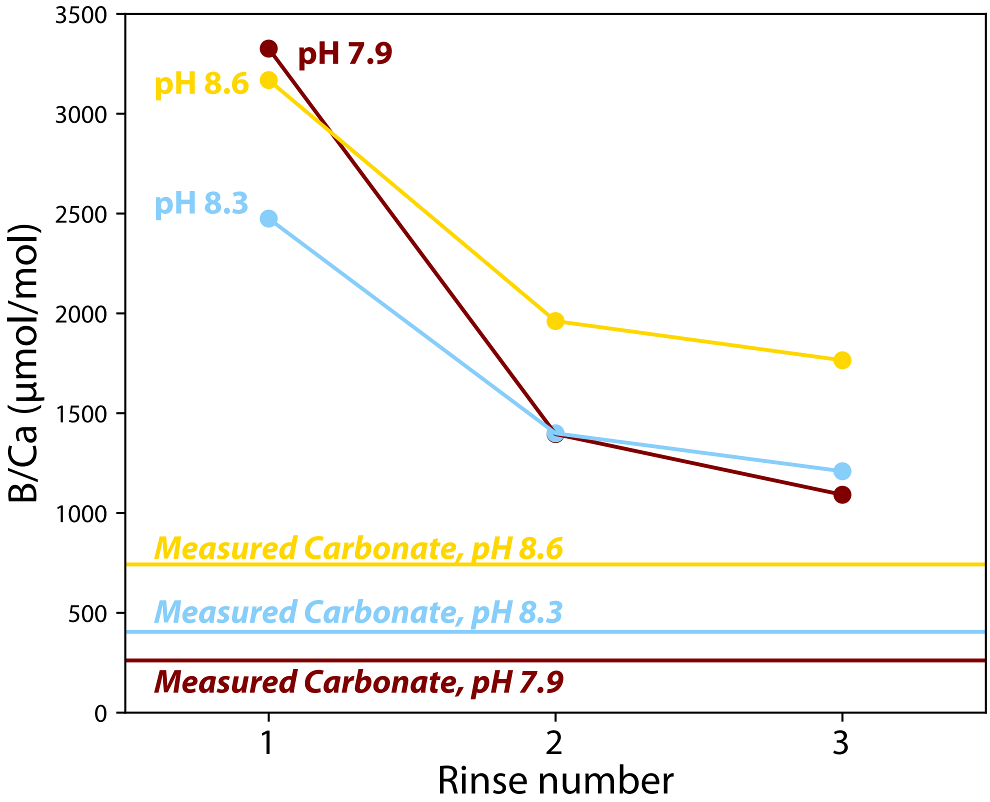

Fig A1: After 3 Milli-Q rinses, substantial excess B relative to the concentration in the eventual carbonate measured was still being removed from the calcite surface.

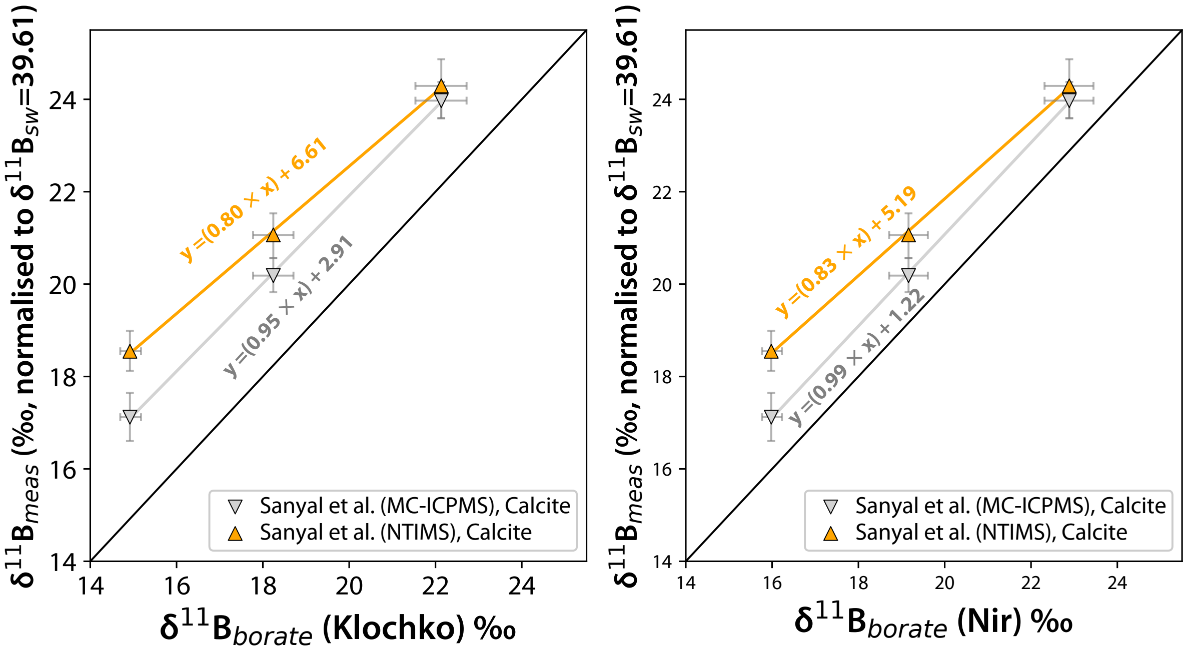

Fig A2: Comparison of measurements of Sanyal et al. (2000)'s calcite precipitates measured via NTIMS and via MC-ICPMS. On the left, the aqueous fractionation factor assumed is 1.0272 (Klochko et al. 2006), and on the right, 1.026 is assumed instead (Nir et al. 2015).

Supplementary Appendix 2: X-ray Diffraction analyses of $CaCO_3$ precipitates

Below are XRD Spectra measured from our experimental precipitates, with representative spectra of calcite (red) and aragonite (blue) shown together for comparison. With the possible exception of sample iMH15/DEC512-D, where a trace presence of calcite is perhaps indicated by a small peak around 29.5˚, all samples appear to be purely one polymorph. For calcite samples, additional unlabelled lines in the final plot are carbonates not precipitated for this study.

Broad humps in the background represent amorphous scattering or fluorescence, likely stemming from the grease/glass used to mount the powder sample. 4 detector positions were used to obtain the range from 3-98° in 2θ. Since the centre of the detector was slightly closer to the sample than the edge, it picked up more intensity. As a result, scattering produces four broad background humps, each corresponding to a detector frame.

For some samples (iMH4/Aug3012E, iMH6/Oct2912E and iMH14/Oct2912E2) an additional peak is seen at ~18˚, and with a weaker secondary peak sometimes evident at ~31.5˚. The most likely candidate for this phase is C_2F_4 *in PTFE (i.e. Teflon), which is the material of the reaction vessel, the suspended magnetic stirring bar, and Teflon tape used to cover injection capillary tubing. Note that any Teflon that might have remained in the sample material after cleaning would not have been dissolved in 0.5 M* HNO_3*, and therefore could not have contributed to our geochemical data.*

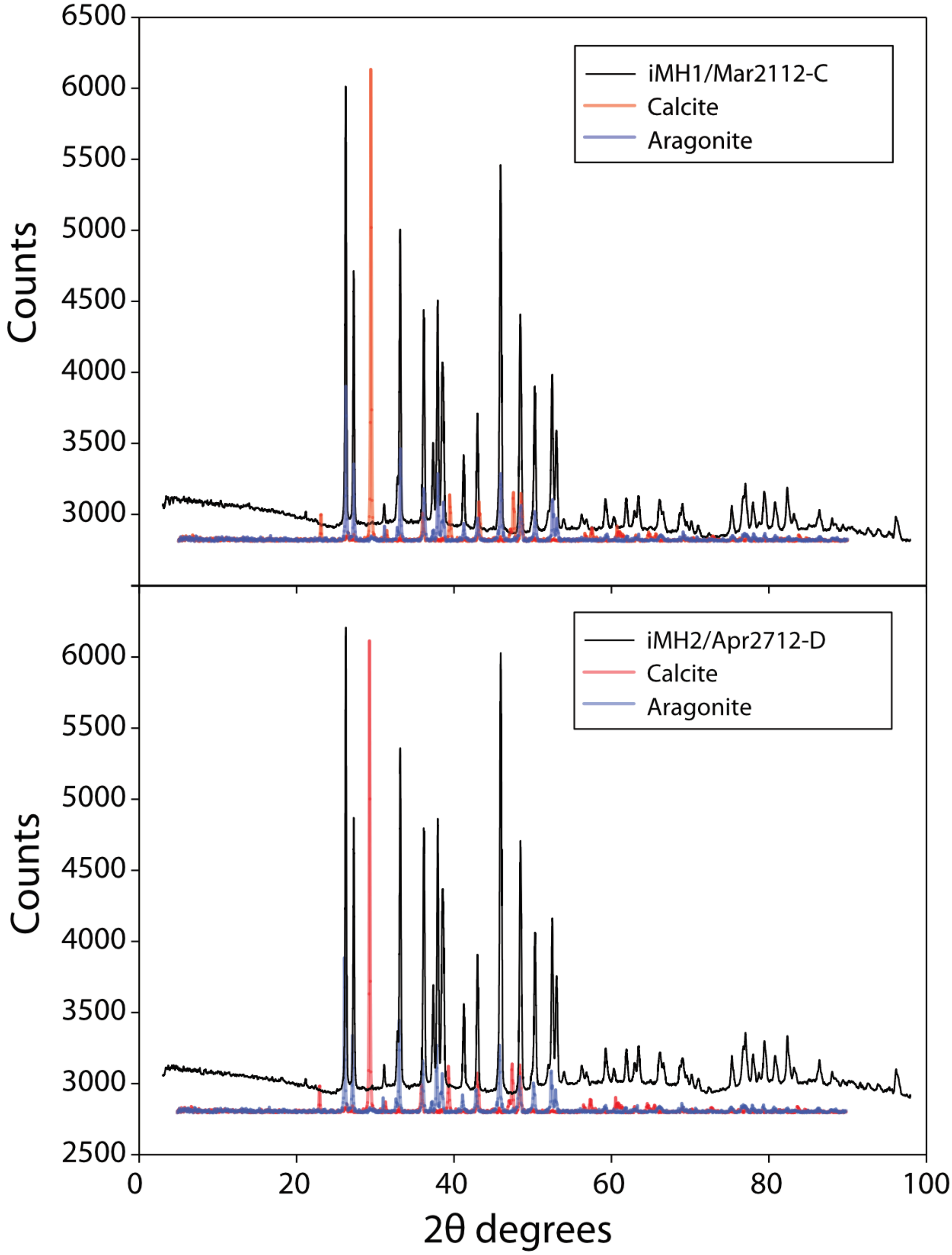
Counts
6500
6000
5500
5000
4500
4000
3500
3000
iMH1/Mar2112-C
Calcite
Aragonite
Counts
6000
5500
5000
4500
4000
3500
3000
2500
iMH2/Apr2712-D
Calcite
Aragonite
0
20
40
60
80
100
2θ degrees

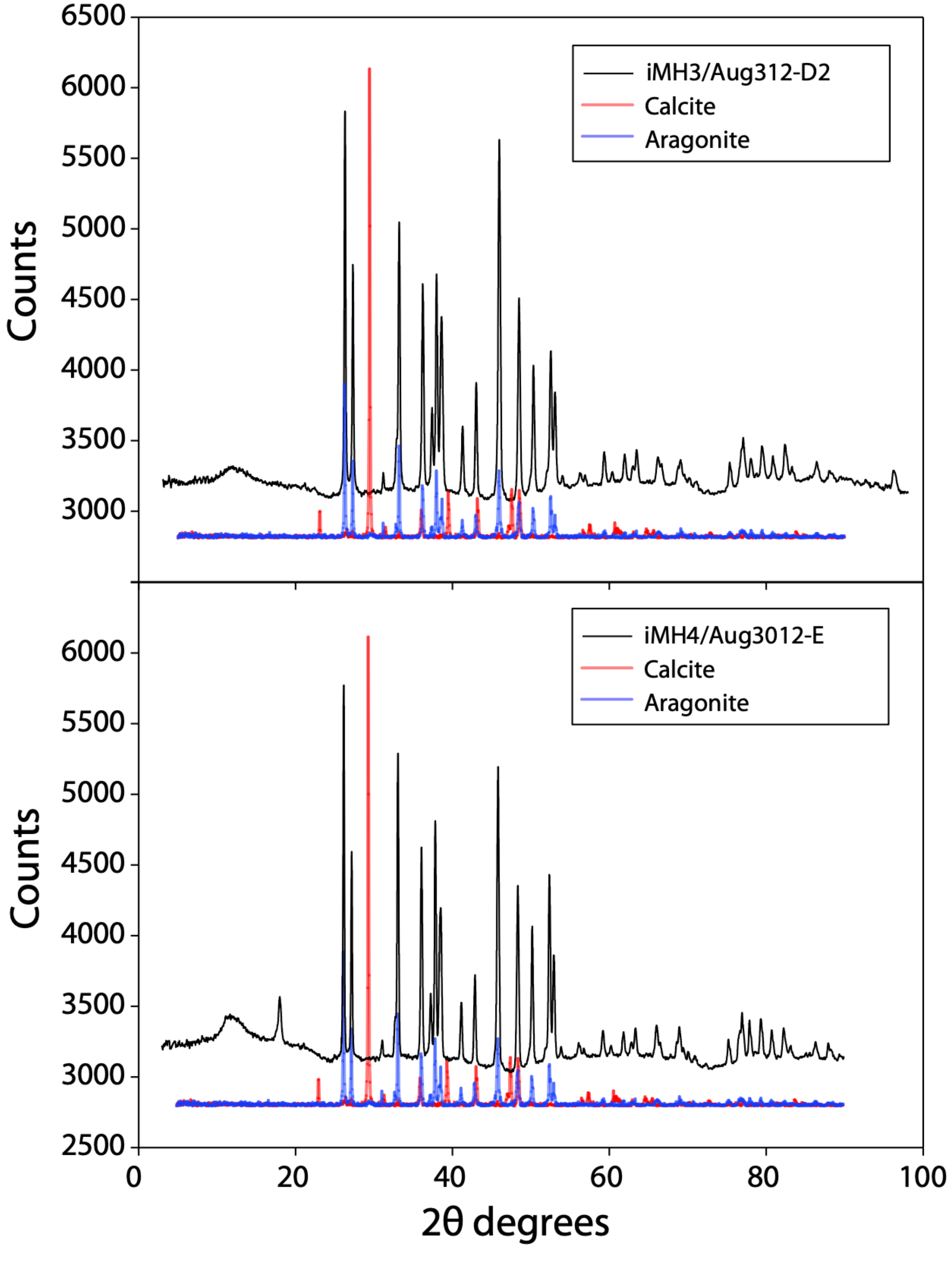
Counts
6500
6000
5500
5000
4500
4000
3500
3000
iMH3/Aug312-D2
Calcite
Aragonite
Counts
6000
5500
5000
4500
4000
3500
3000
2500
iMH4/Aug3012-E
Calcite
Aragonite
0
20
40
60
80
100
2θ degrees

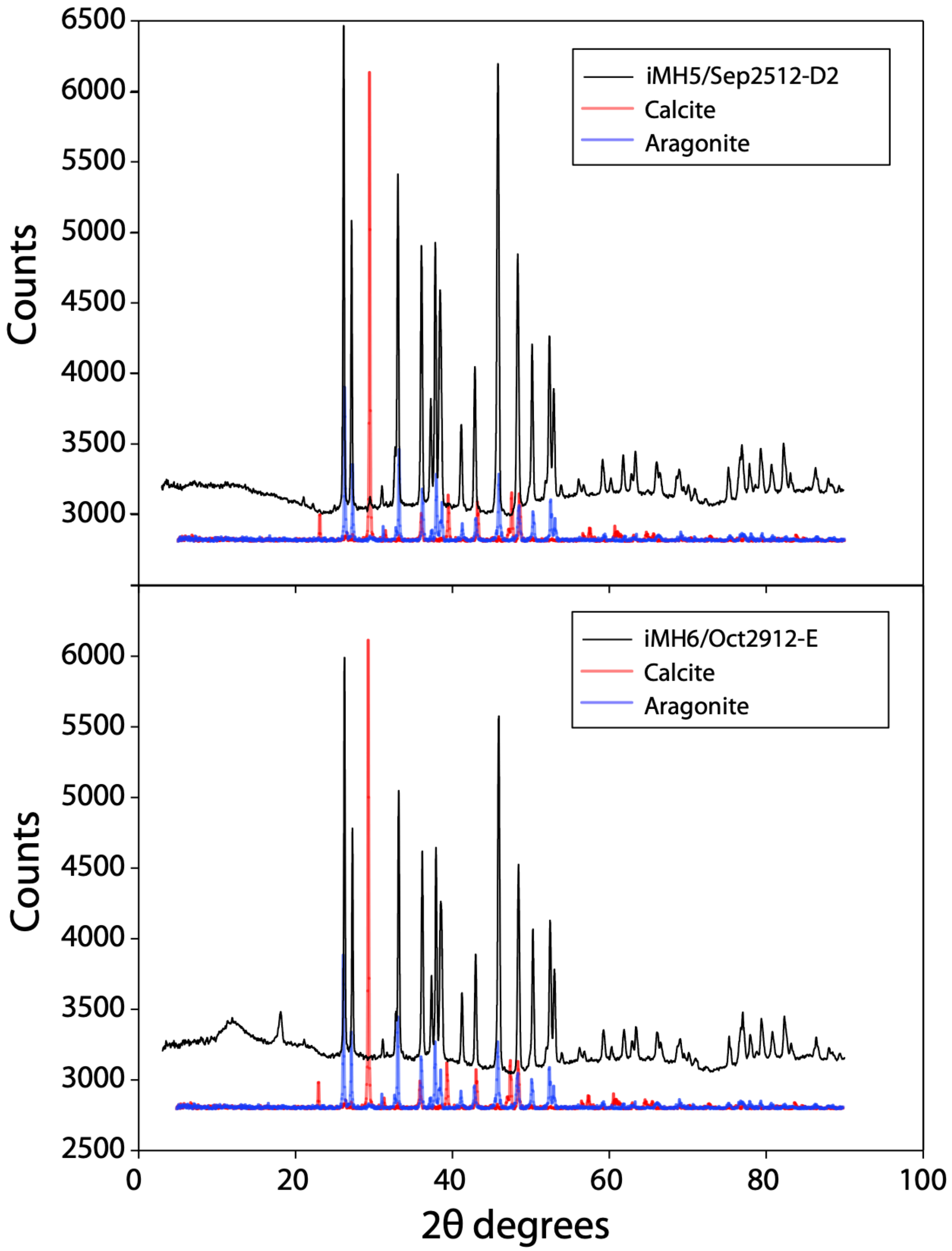

6500
6000
5500
5000
4500
4000
3500
3000
Counts
iMH5/Sep2512-D2
Calcite
Aragonite
6000
5500
5000
4500
4000
3500
3000
2500
Counts
iMH6/Oct2912-E
Calcite
Aragonite
0
20
40
60
80
100
2θ degrees

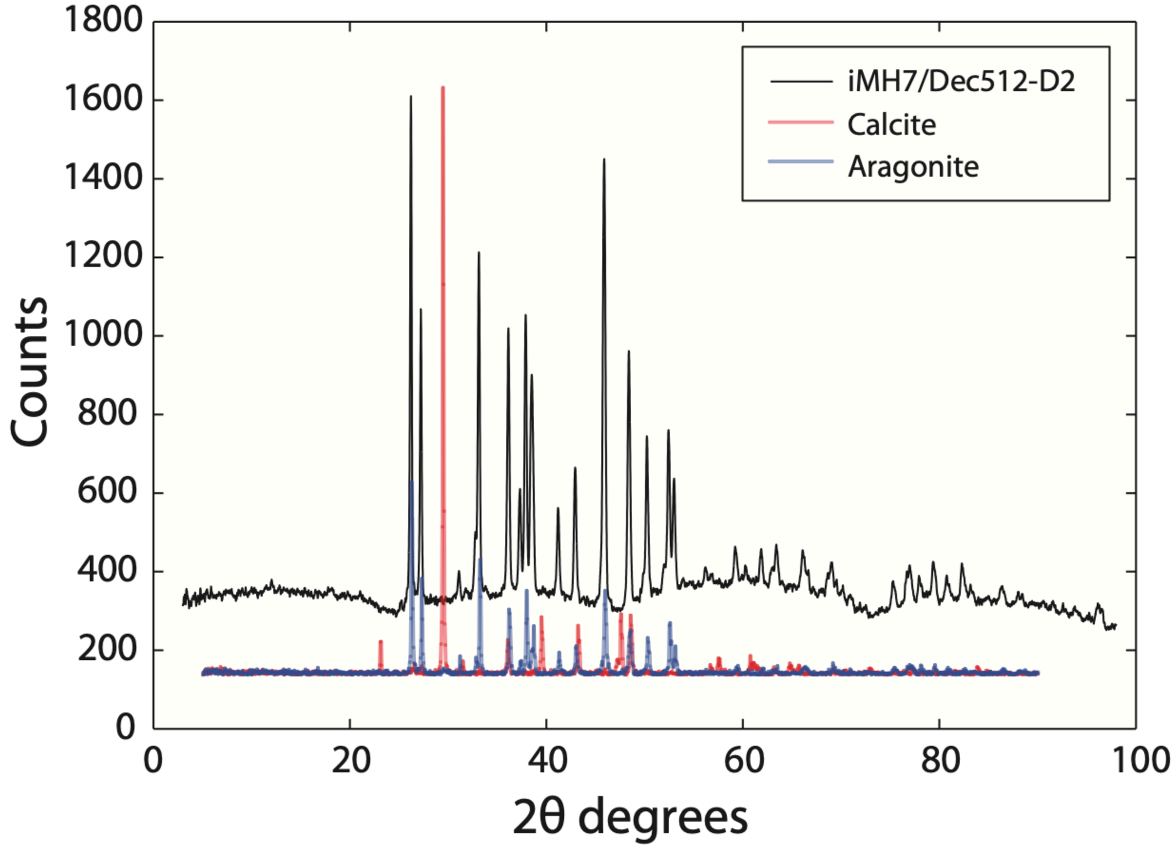
1800
1600
1400
1200
1000
800
600
400
200
0
Counts
0
20
40
60
80
100
2θ degrees
iMH7/Dec512-D2
Calcite
Aragonite

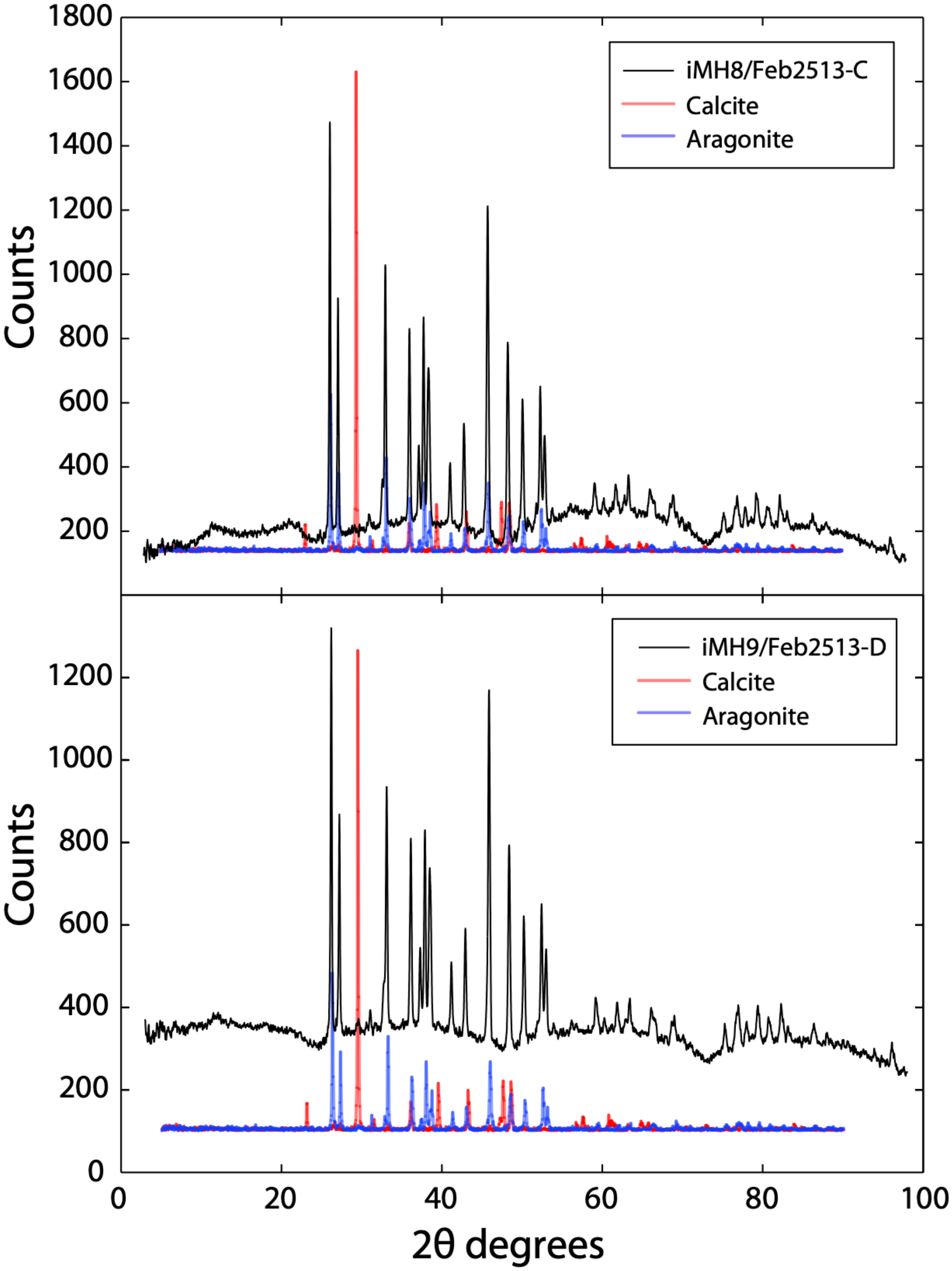
1800
1600
1400
1200
1000
800
600
400
200
Counts
iMH8/Feb2513-C
Calcite
Aragonite
1200
1000
800
600
400
200
0
Counts
iMH9/Feb2513-D
Calcite
Aragonite
0
20
40
60
80
100
2θ degrees

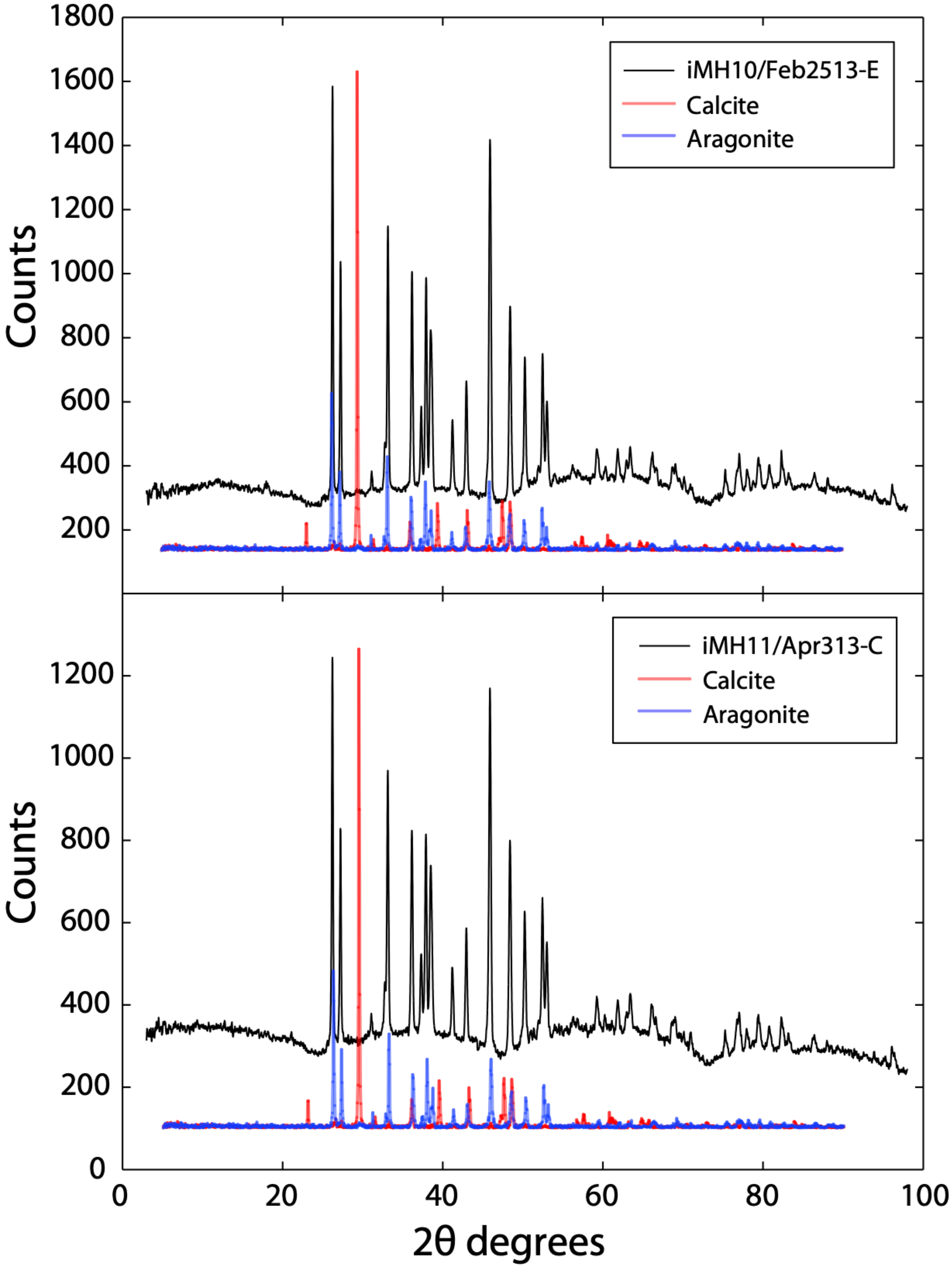
Counts
1800
1600
1400
1200
1000
800
600
400
200
iMH10/Feb2513-E
Calcite
Aragonite
Counts
1200
1000
800
600
400
200
0
iMH11/Apr313-C
Calcite
Aragonite
0
20
40
60
80
100
2θ degrees

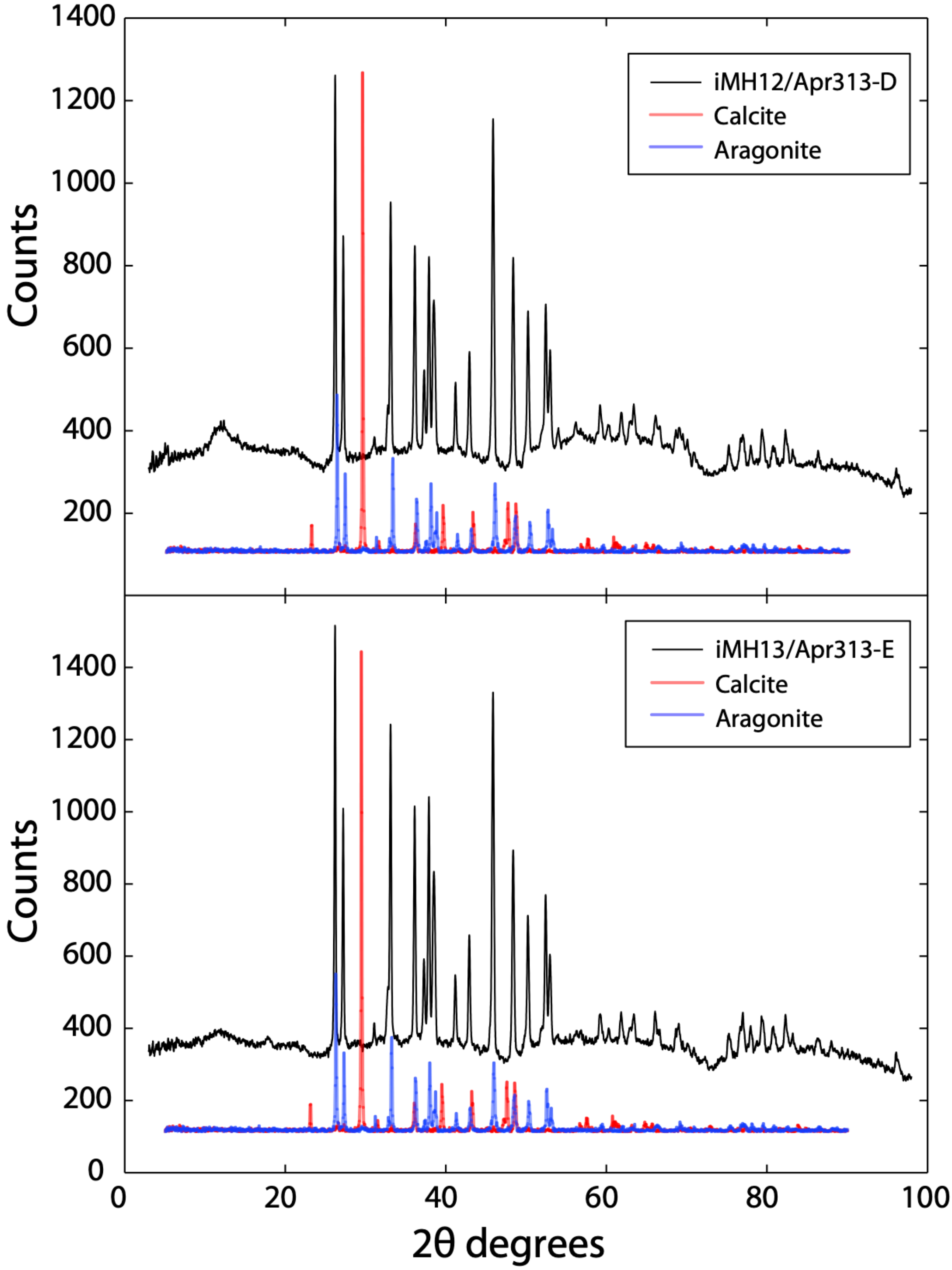

Counts
1400
1200
1000
800
600
400
200
iMH12/Apr313-D
Calcite
Aragonite
Counts
0
200
400
600
800
1000
1200
1400
iMH13/Apr313-E
Calcite
Aragonite
0
20
40
60
80
100
2θ degrees

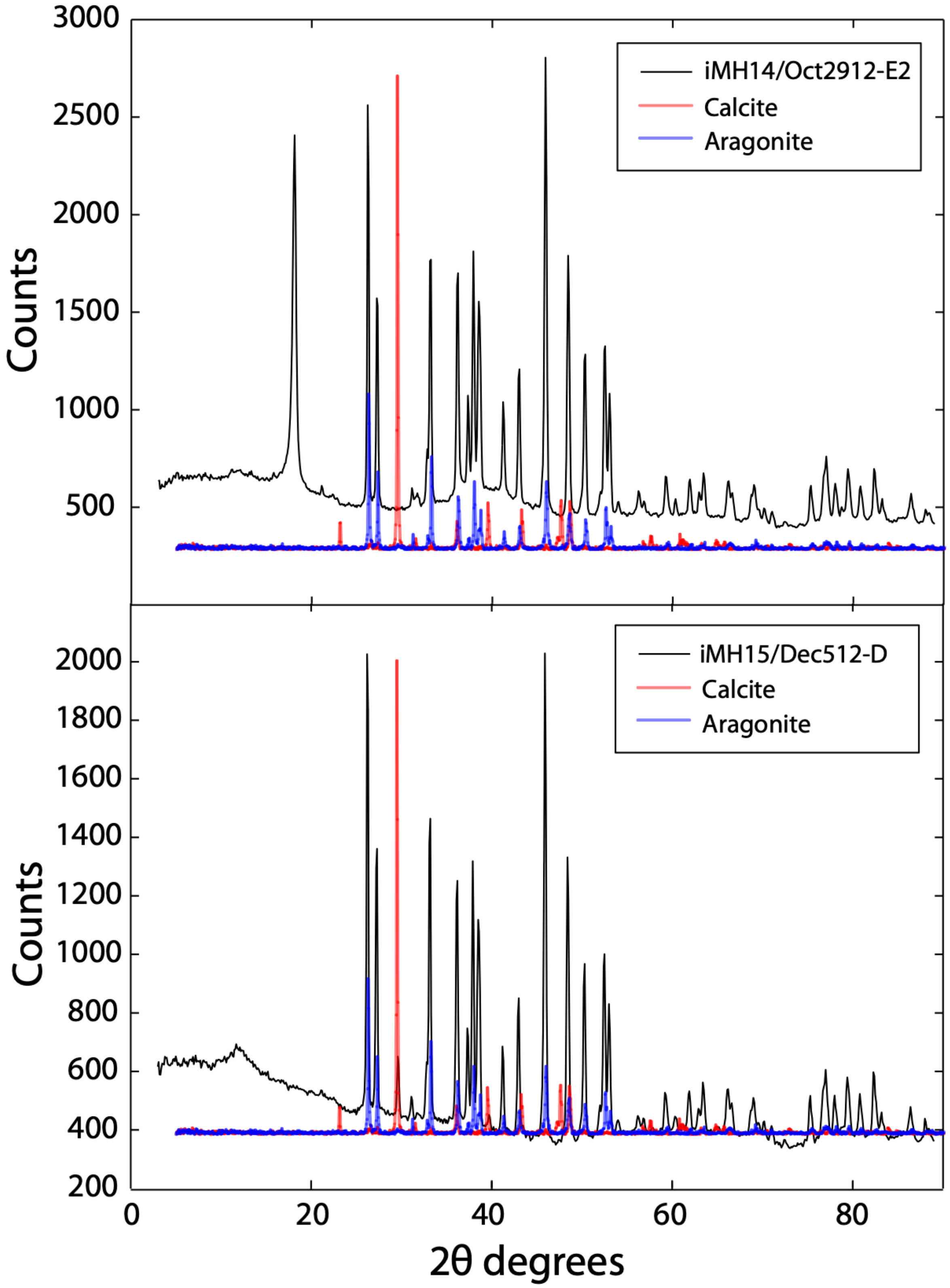
iMH14/Oct2912-E2
Calcite
Aragonite
Counts
3000
2500
2000
1500
1000
500
iMH15/Dec512-D
Calcite
Aragonite
Counts
2000
1800
1600
1400
1200
1000
800
600
400
200
0
20
40
60
80
2θ degrees

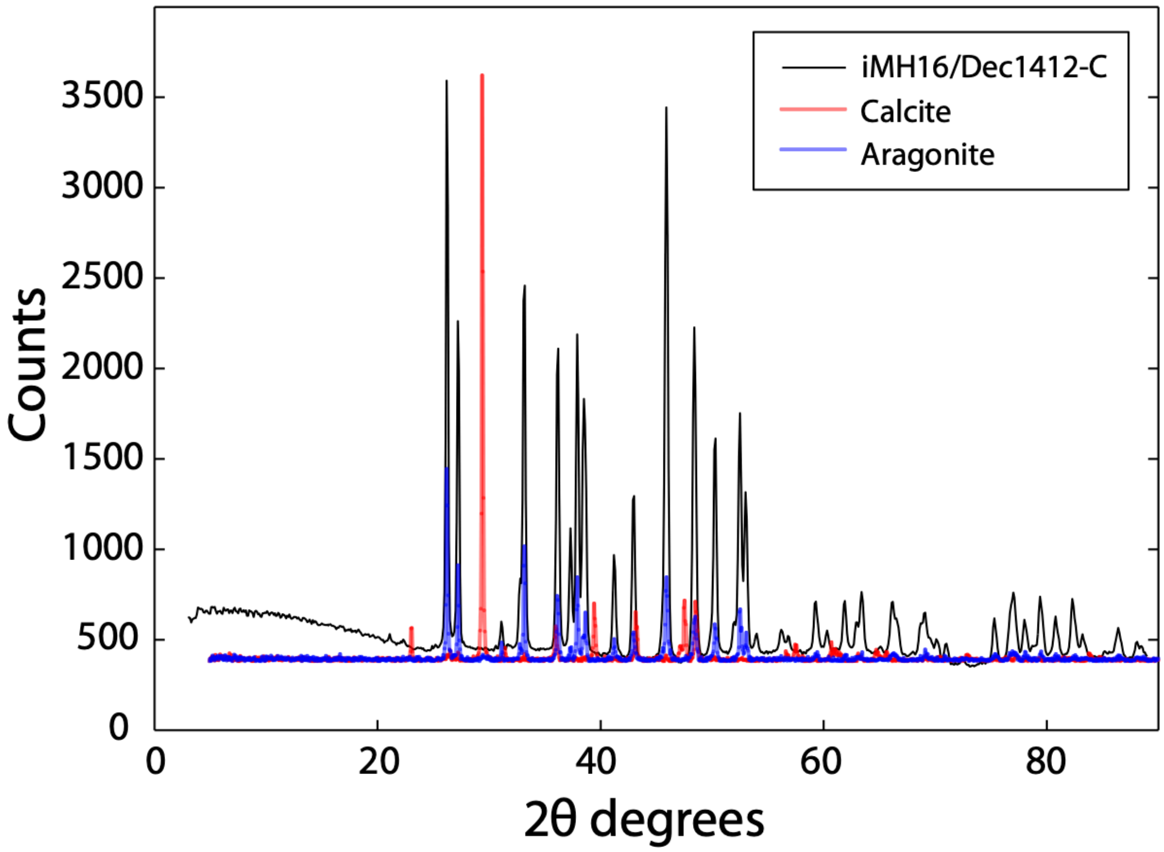
iMH16/Dec1412-C
Calcite
Aragonite
Counts
0
500
1000
1500
2000
2500
3000
3500
0
20
40
60
80
2θ degrees

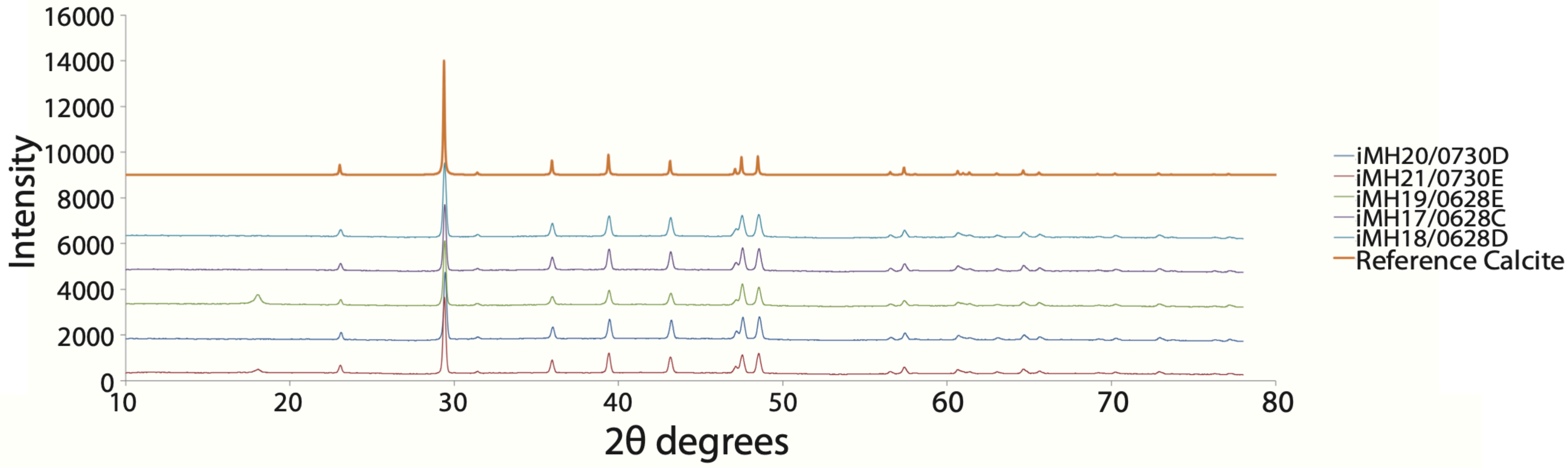
16000
14000
12000
10000
8000
6000
4000
2000
0
Intensity
10
20
30
40
50
60
70
80
2θ degrees
iMH20/0730D
iMH21/0730E
iMH19/0628E
iMH17/0628C
iMH18/0628D
Reference Calcite

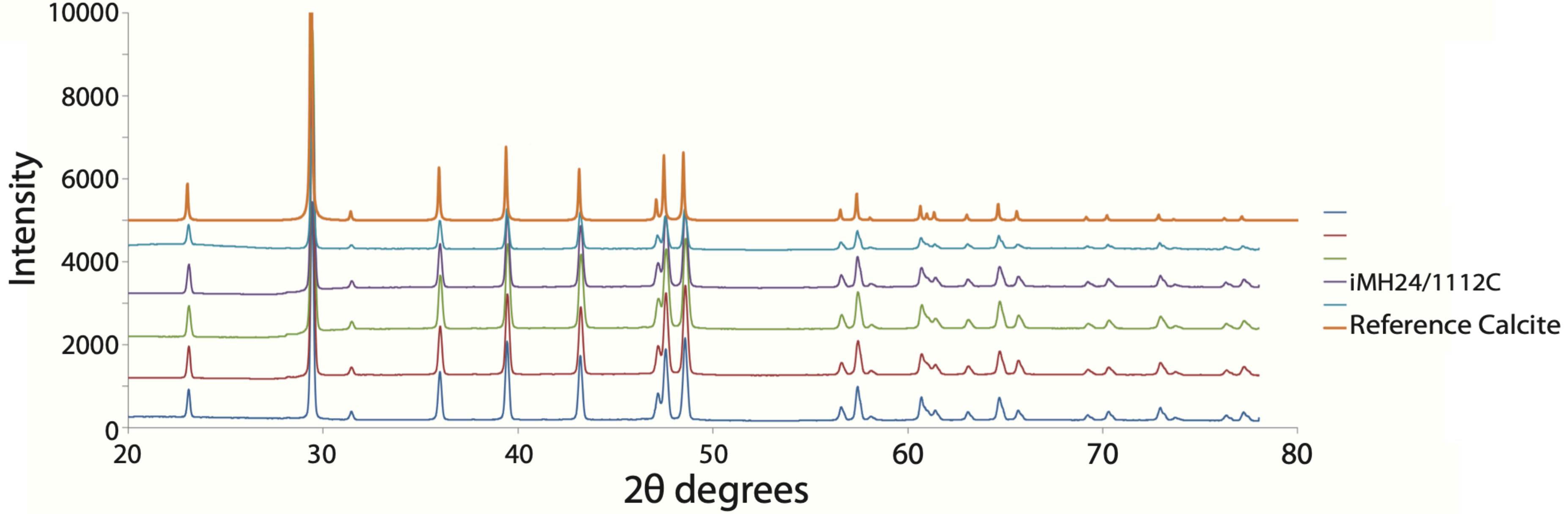
10000
8000
6000
4000
2000
0
Intensity
20
30
40
50
60
70
80
2θ degrees
iMH24/1112C
Reference Calcite